Development of a model burner for turbulent premixed hydrogen-air combustion at high exhaust gas recirculation (EGR) rates

M. Schneider[1], M. Bauer[1], S. Schulz[1], P. Habisreuther[1], C. Weis[1], B. Stelzner[1*], D. Trimis[1]

*bjoern.stelzner@kit.edu

[1]*Engler-Bunte-Institute, Division of Combustion Technology, Karlsruhe Institute of Technology, Karlsruhe, Germany*

Abstract

The combustion properties of hydrogen are very different from those of conventional hydrocarbons. One of these is the high burning velocity of hydrogen flames. In addition, high diffusion rates in the flame region lead to very short reaction zones and to thermo-diffusive flame instabilities. These reasons lead to the fact that hydrogen is usually not combusted premixed in technical systems due to operational safety. On the one hand, this causes locally high temperatures and thus promotes the formation of increased nitrogen oxide contents in the exhaust gas, and on the other hand, this severely restricts the operating ranges and controllability of technical applications.

In the premixed system, there is also a risk of flashback, which increases when pure hydrogen is used as fuel due to the increased diffusivity and flame speed combined with a reduced quenching distance. To avoid flashback and to meet the necessary operational safety requirements, suitable mixing concepts must be used. Fuel gas and air are fed separately into the mixing module and are mixed. The requirements for the mixing module are to ensure a high mixing quality with short residence times and short mixing distances, in order to avoid local formation of layers and thus changes in the stoichiometry. In addition, the pressure loss during mixing must be kept as low as possible so that no complex blower equipment is required for operation and thus conventional peripherals can be used.

The object of the presented research is the premixed combustion of hydrogen-air flames mixed with cooled recirculated exhaust gas, which leads to increased flame stability. In addition, the reaction zone is stretched by the intelligent flow control in order to generate a homogeneous, extended heat release zone as a basis for heat extraction from the combustion system in technical systems, especially for industrial applications. For the investigations, a model burner is developed and parametrically investigated with respect to premixing, exhaust gas recirculation rate and combustion staging.

From these fundamental studies, mixing and combustion concepts are derived that allow safe premixed hydrogen combustion similar to operation with burner technologies for conventional hydrocarbons. In addition to stabilizing and stretching the combustion process, the focus is on minimizing nitrogen oxide emissions.

As part of the research, a modular model burner was developed to investigate turbulent, premixed hydrogen-air combustion at high exhaust gas recirculation rates. The model burner consists of a central primary nozzle surrounded by a secondary nozzle and an outer co-flow jacket. The hydrogen-air and exhaust gas mixture is injected through the primary nozzle, which is designed to form a flat flow profile. The secondary nozzle allows fuel staging with and without swirl. The outer co-flow jacket avoids recirculation areas of hot flue gas.

The experimental work was performed using laser spectroscopic methods to determine velocity flow fields for selected operating points with air under Reynold's law of similitude assumptions. In this case, the high-speed particle image velocimetry (PIV) was used to experimentally determine the global velocity field. This information was used to validate the numerical model in the non-reactive case. To select the operating range in the reactive case, the laminar burning velocity of hydrogen-air with different content of exhaust gas admixture was studied using the heat-flux-method. Based on these results, the reaction regions of the model burner setup were investigated.

Introduction

With the ongoing decarbonisation of the energy market, it can be assumed that hydrogen will be widely available in the near future and will play an important role in end-use applications [1]. In addition to the use of synthetic hydrocarbons produced from "green" hydrogen, the combustion of carbon-free chemical energy sources is an attractive option for avoiding CO_2 emissions. In this context, hydrogen produced by water electrolysis for the storage of excess renewable electricity can be used as a primary energy carrier [2]. However, conventional burner systems are often not suitable for operation with pure hydrogen due to its combustion characteristics. There is therefore a need for new developments that are designed for operation with pure hydrogen when process heat is required. In current studies, the focus is on hydrogen-enriched methane flames [3,4] and is slowly shifting towards pure hydrogen combustion. The combustion properties of hydrogen differ greatly from those of conventional hydrocarbons. In this context, the high burning velocity of hydrogen-air flames of about 320 cm/s with an air factor of 0.6 should be mentioned [5]. Furthermore, high diffusion rates in the flame area lead to very short reaction zones and to thermo-diffusive flame instabilities [6].

These reasons mean that hydrogen is not premixed in today's technical systems for reasons of operational safety. On the other hand, non-premixed combustion leads to locally high peak temperatures and thus promotes the formation of nitrogen oxides in the exhaust gas, which also severely restricts the operating ranges and controllability of technical applications. In a premixed system, there is also the risk of flame flashback [7,8], which increases greatly when pure hydrogen is used as fuel due to the increased diffusivity and flame velocity in combination with a reduced quenching distance. Due to the reduced quenching distance, hydrogen-air flames propagate closer to the walls before extinguishing than other fuels. In automotive engines, this significantly increases the tendency to misfire, as the hydrogen-air mixture passes closer to the intake valve than hydrocarbon flames [9]. Hydrogen engines are also characterised by higher NOx concentrations compared to hydrocarbon fuels [10].

To solve these problems in the context of hydrogen-air combustion, dilution with steam or nitrogen is often used [11]. The experimental and numerical results of Lu et al. [12] showed that NO emissions from steam dilution are about 20-50% of those from N_2 dilution at the same equivalence and dilution ratio, which is due to the direct chemical and third-body effects of steam that reduce the formation of NO mainly in the NNH pathway.

Another way to better control the combustion of premixed hydrogen is to recirculate exhaust gas. Currently, the concept of exhaust gas recirculation (EGR) is mainly used in spark ignition engines [13,14] or turbines [15]. It is one of the key technologies for pure hydrogen combustion as it can reduce NO_X emissions [16,17]. EGR acts as an additional diluent in the unburned gas mixture and lowers peak combustion gas temperatures and NO_X formation rates [18], provided an adequate amount of heat is removed from the exhaust gases. Furthermore, measurements on a spherically expanding flame at constant pressure carried out by Duva et al. [19] showed that the flame velocity and adiabatic flame temperature decrease almost linearly with increasing degree of dilution by EGR. This effect was demonstrated by Wang et al. [20].

Turbulent H_2-flame configurations are usually in co-flow configuration and different stabilisation concepts such as piloting, use of bluff bodies or swirl are applied. Established and well-studied H_2 (+ blends) non-premixed model flames can be found e.g. in [21],[22],[23] and are collected in the TNF workshop.

The length of non-premixed hydrogen jet flames L_F was given by Molkov and Saffers in [24]. Depending on the nozzle diameter d, the ratio L_F/d was between 100 and 200 for Reynolds number above 10,000. For premixed hydrogen jet flames, however, a much smaller flame length is expected. Kwon et al. [25] showed the dependency of Reynolds number and equivalence ratio on the L_F/d ratio, which is between 1.9 and 11.7. In this work, the development and design of a model burner for turbulent premixed hydrogen-air flames at high exhaust gas recirculation (EGR) rates are presented. Furthermore, the turbulent flow fields are investigated experimentally and numerically.

Preliminary study for design

The numerical study was carried out using ANSYS ChemkinPro 21 package to investigate premixed hydrogen-air flames with EGR. In the parametric study of freely propagating 1D flames, the equivalence ratio ($0.3 < \Phi < 3.0$), inlet temperature (300 K to 673 K) and EGR (0 to 1) were varied over a wide

range. The simulations were conducted using the Konnov mechanism from 2019 [26]. Equation (1) shows the definition of the exhaust gas recirculation rate EGR as the fraction of the mass flows.

$$EGR = \frac{\dot{m}_1}{\dot{m}_2} \tag{1}$$

The first calculation series investigates the pure influence of recirculation rate using as a maximum estimation that the temperature of the recirculated flow is reduced to the preheating temperature Tin. Figure 1 illustrates for this assumption the generation of inlet conditions for the laminar flame calculations with maximum heat loss. In a first stream, fresh H_2-air mixture is used with air factor λ, pressure p and the inlet temperature Tin. The composition of a second stream is calculated using the equilibrium code of ANSYS Chemkin Pro for the same mixture, but restricting the possible species-set to the components H_2, O_2, N_2 and H_2O. The resulting mixture composition and temperature T_{eq} of this pseudo-equilibrium is then artificially set to the inlet temperature Tin of the first mixture. The inlet conditions for the 1D hydrogen flame calculation is then calculated by a mass flow weighted mixture of the two described streams.

In the calculation series, the pure influence of the recirculation rate was investigated, assuming as a maximum assumption that the temperature of the recirculated stream is reduced to the preheating temperature T_{in}. Figure 1 illustrates for this assumption the generation of inlet conditions for the laminar flame calculation with maximum heat loss. In a first stream, $\dot{m}_1$ fresh H_2-air mixture with air factor λ, pressure p and inlet temperature T_{in} was used. The composition of a second stream $\dot{m}_2$ was calculated using the equilibrium code of ANSYS Chemkin Pro for the same mixture, limiting the possible species to the components H_2, O_2, N_2 and H_2O. The resulting mixture composition and temperature T_{eq} of this pseudo-equilibrium was then artificially set to the inlet temperature T_{in} of the first mixture. The inlet conditions for the 1D hydrogen flame calculation were then calculated by a mass flow weighted mixture of the two flows described. The calculation scheme is illustrated in Figure 1.

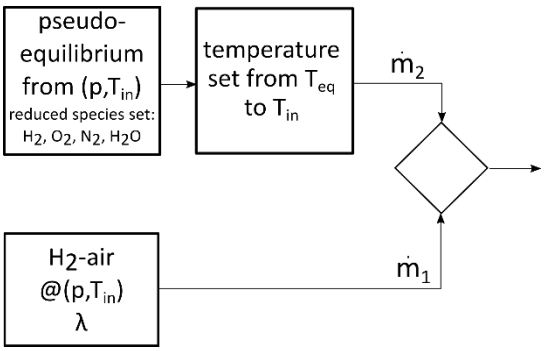

Figure 1. Sketch illustrating the generation of inlet conditions for laminar flame calculations with maximum heat loss.

Figure 2 shows the laminar flame speed of hydrogen-air flames in cm/s as a function of the air factor λ for an inlet temperature of 300 K on the left and for an inlet temperature of 673 K on the right. The results show the laminar flame burning velocity versus air factor between $0.3 \leq \lambda \leq 3.0$ when varying the EGR rate from 0 (in black) to 1.0 (in red) in 0.2 steps. In addition, the fresh gas inlet temperatures were varied (300 K, 373 K, 473 K, 573 K and 673 K). The diagrams show the inlet temperatures of 300 K and 673 K as examples.

The maximum laminar burning velocity for both diagrams at an EGR ratio of 0.0 is about 320 cm/s for an air factor of $\lambda = 0.6$ in the left diagram and about 1140 cm/s for an air factor of $\lambda = 0.55$ in the right diagram. After reaching the maximum, the laminar burning velocity decreases with increasing air factor. For both inlet temperatures it results that laminar burning velocity decreases with increasing EGR rate and the maximum is shifted towards higher air factors. For an EGR rate of 1.0 and an inlet temperature of 300 K, the maximum flame speed of about 60 cm/s is reached at an air factor of $\lambda = 0.75$. For an inlet temperature of 673 K and an AGR rate of 1.0, the maximum flame speed of about 480 cm/s is achieved with an air factor $\lambda = 0.65$. The shift to higher air factors with increasing EGR rate is more

pronounced at lower inlet temperatures, and at higher inlet temperatures the maximum flame speed shifts slightly to lower air factors.

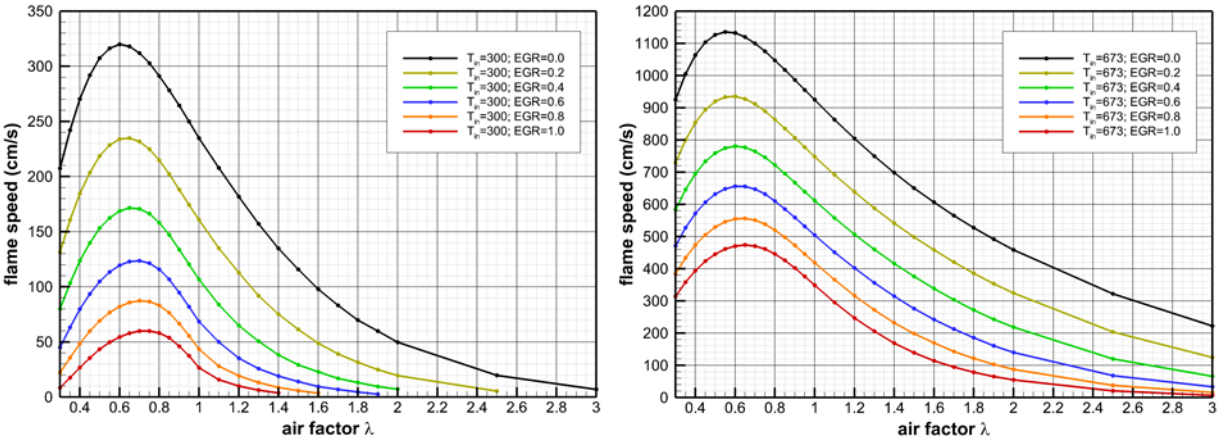

Figure 2. Flame speed of hydrogen-air flames in cm/s as function of the air factor λ for inlet temperature of 300 K (left) and 673 K (right) for different EGR rates (0, 0.2, 0.4, 0.6, 0.8, 1.0) (p_0 = 1 bar).

In the present study, the concept of combustion with EGR is to keep the laminar flame speed almost constant. As a results, the air factor λ must be reduced with increasing EGR. In the case of pure hydrogen air combustion (EGR = 0), the air factor is λ = 2.0. This condition is mainly used for the design of the burner characteristics.

Model Burner Design

The burner consists of three circular inlets in co-flow configuration: the inner inlet, the inner ring and an outer co-flow. The inner inlet is design as a contracting nozzle according to DIN ISO EN 5167-3 to create a flat velocity profile at the outlet. One outlet diameter before the contraction, a coarse mesh (mesh size = 1.7 mm, wire thickness = 0.4 mm) was placed to induce turbulence. The inner ring (gap width = 10 mm) also contracts constantly with its flow through area to achieve same effect. In addition, a swirl body can introduced into this flow. However, it was not used in the present study. Both nozzle design features lead to a suboptimal inflow of the co-flow. Here, a sintered plate with a thickness of 6 mm and low porosity (about 25%, pore size = 1.1 µm) is placed to force homogenous distribution due to high pressure losses. The combustion chamber is designed rectangular with a width of 160x160 mm and a height of 300 mm, allowing full optical access as well seven ports for invasive measurements. The burner design is shown in Figure 3 and the burner setup in Figure 4.

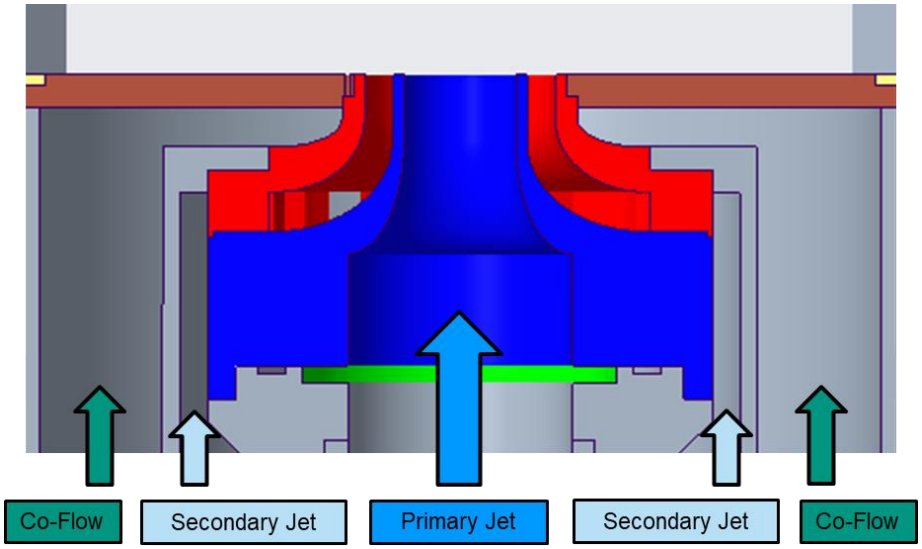

Figure 3. Design of the nozzle burner.

Inlet diameter of the primary jet is 40 mm and contracts to 20 mm at its exit. The secondary jet shows an inner diameter of 24 mm and an outer diameter of 34 mm. The co-flow has a total diameter of 150 mm. The length of the combustion chamber (see Figure 4) is 300 mm.

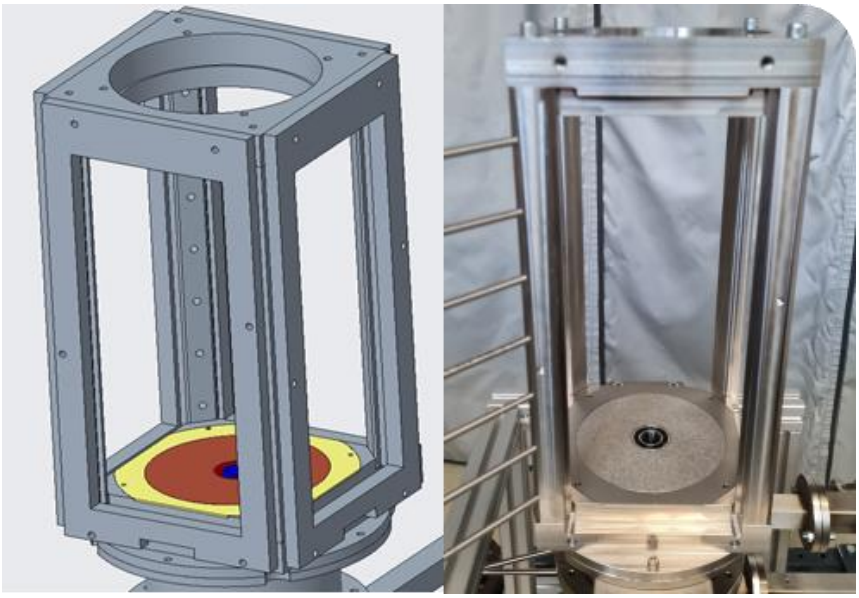

Figure 4. Design of the combustion chamber (left: CAD, right: photo).

The velocity gradients at boundary were used to determine the operating range to avoid flashback and blow-off. A hydrogen-air flame with an equivalence ratio of $\Phi = 0.5$, which corresponds to a laminar burning velocity of $s_L = 50$ cm/s, contains about 17 % hydrogen by volume. For this boundary conditions, the velocity gradient must be $g > 2{,}000\ s^{-1}$ to avoid flashback and $g < 100{,}000\ s^{-1}$ to avoid blow-off according to von Elbe and Menster [27].

Table 1. Theoretical operation limits.

	Based on	Flash back	Operation	Blow-off
g in 1/s	H_2 + air, $\Phi = 0.5$	2,000	28,700	100,000
Re	H_2 + air, $\Phi = 0.5$	2,300	10,000	20,000
u_{mean} in m/s	H_2 + air, $\Phi = 0.5$	3.6	15.8	31.6
u_{exp} in m/s	air	1.8	7.9	15.8
P in kW	H_2 + air, $\Phi = 0.5$	1.9	8.5	16.9

Wu et al. reported flame lengths for turbulent premixed hydrogen/air flames at high Reynolds number in [25]. The length depends highly on equivalence ratio and the Reynolds number and showed values of $1.9 < L_f/d < 11.7$ for the investigated boundary conditions. For the suggested operation case (see Table 1), the expected flame length is about 4 to 5 times the nozzle diameter of the jet. In [22], Wu et al. have given flame lengths for turbulent premixed hydrogen/air flames at high Reynolds numbers. The length strongly depends on the equivalence ratio and the Reynolds number and resulted in values of $1.9 < L_f/d < 11.7$ for the investigated boundary conditions. For the proposed operating case (see Table 1), the expected flame length is about four to five times the nozzle diameter of the jet. The investigated cases are shown in Table *2*. The study focuses on the both central jets and the co-flow was not used.

Table 2. Investigated cases.

	Jet 1			Jet 2		
Case	Re	u in m/s	$\dot{m}$ in kg/s	Re	u in m/s	$\dot{m}$ in kg/s
1	10,000	7.9	0.002936735	10,000	16	0.002936735
2	10,000	7.9	0.008625044	5,000	8	0.004312522

Numerical Approach

Computational fluid dynamics simulations were performed by Reynolds-averaged Navier–Stokes (RANS) equations numerical calculations using the rhoSimpleFoam solver of OpenFOAM 5.0. The computational domain was discretized as a finite volume mesh consisting of 522,521 cells. The cell size, in terms of the cube root volume, varies between approximately 0.136 mm and 4.786 mm, ensuring sufficient resolution of geometrical features. The domain includes the combustion chamber and the nozzle up to 52 mm upstream of combustion chamber. The mean cell size in the combustion chamber was 4.463 mm consisting of mainly hexahedra cells.

The calculations were carried out with a k-ε model. The turbulent boundary conditions were set to a turbulence intensity of 10 % for kinetic turbulent energy (k) and mixing length (0.4 mm for the central jet and 0.28 mm for the secondary inlet) based estimation for the dissipation rate (ε). Mixed wall functions for low- and high-Reynolds number were applied for k and ε and for turbulent viscosity a velocity-based wall function using Spalding's law was applied.

The fluid was modelled as a perfect gas with a molar weight of 28.96 g/mole and a heat capacity of 1.006 J/g/K. Transport coefficients were calculated based on the Sutherland transport model with a reference viscosity of $1.4584*10^{-6}$ kg/m/s and a reference temperature of 110.33 K.

The simulations were carried out for two different operating conditions as shown in Table 2. The calculations were performed until stationary results were achieved at residuals for momentum, k and ε below $1*10^{-4}$ where no significant changes in pressure and velocity were observable between iterations.

Experimental Approach

Two-dimensional flow fields for the different inlet boundary conditions were determined using particle imaging velocimetry (PIV). The basics of the measurement technique are described in detail in [28].

Using an Nd:YLF double cavity laser (Litron LDY304), two green laser beams two green laser beams were sent through the cylindrical optical system with variable delay to create a light sheet with a height of 130 mm and a thickness of 600 µm ($1/e^2$ radius) at the waist. The experiments were performed at repetition rates at 200 Hz. Each of the two inner streams was seeded with di-ethyl-hexyl-sebacat (DEHS) using a seeding generator (Palas AFG 10) with an average droplet size of approximately 0.5 µm. The scattered light was recorded with a 12-bit CMOS camera (Vision Research Phantom v1212) with a resolution of 1280 x 800 pixels. A Nikon 50 mm f/1.4 lens in combination with narrow-band green filter was used for the recording. The resulting field of view was 120 x 80 mm^2. The camera was aligned perpendicular to the illuminated area. Commercial software (LaVision Davis 10) was used for image acquisition, parameter setting, perspective correction and image correlation. The time delay (Δt = 60 µs) between the double images was determined as a function of the size of the correlation window (32 x 32) and the velocity range of the experiment. A window overlap of 75% was chosen. The independence of the resulting velocity fields from the size of the interrogation window and the time delay Δt was verified in preliminary investigations. As a rule, each measurement series consists of about 1000 vector fields. A statistical analysis was performed near the nozzle exit and showed a statistical error of less than 3 % for the main velocity component and less than 15 % for the rms values (3 σ confidence). The procedure is described in [29].

All streams of the burner were operated with air at ambient temperature and atmospheric pressure. In inlet velocities were set with thermal mass flow controllers.

Results and Discussion

The numerical and experimental results of axial velocity fields are compared in Figure 5 for both cases investigated. The numerical results include the two velocity streams inside the nozzles. Upstream the burner exit, the maximum velocity in the first case is found to be about 16 m/s in the centre of the second jet and almost 8 m/s in the second case. The total length of the jets is between 220 mm and 300 mm, where the flow homogenises. Here, the experiments show a smaller jet length than the simulations, but the main jet structure agrees well with the numerical results.

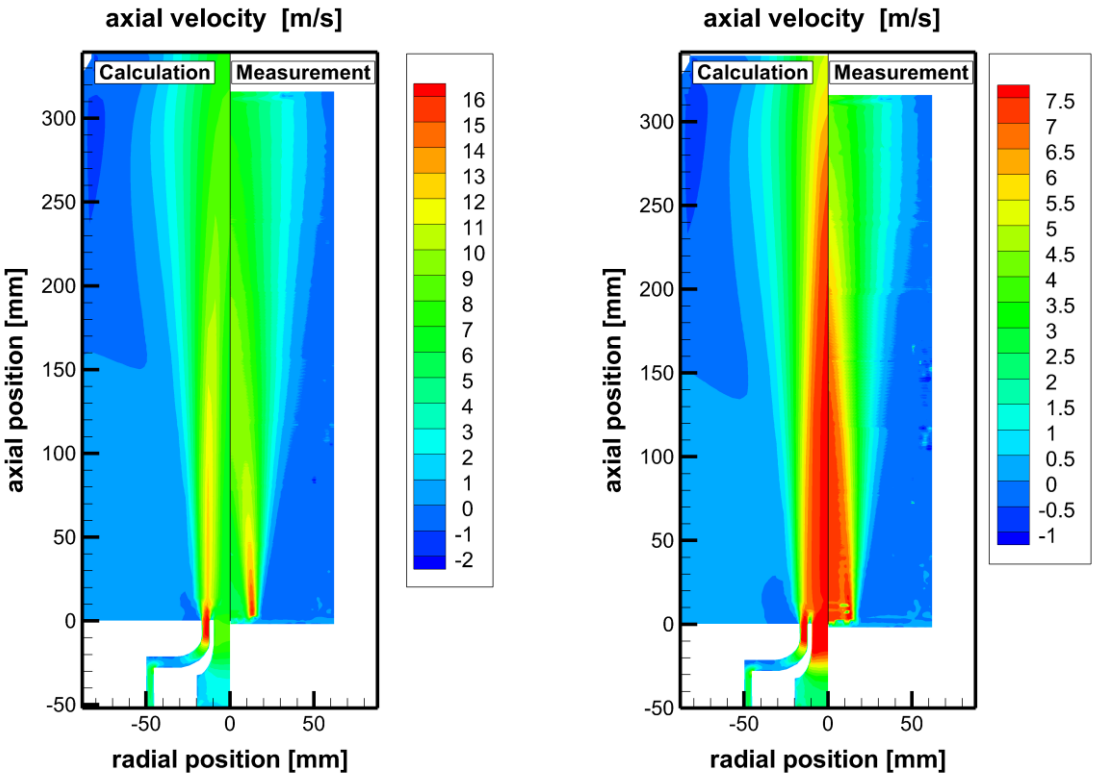

Figure 5. Numerical and experimental results of the axial velocity fields for case 1 (left) and case 2 (right).

Different heights above the burner were selected for further investigations (5 mm, 40 mm, 100 mm and 200 mm respectively, based on the diameter of the inner jet with D_0 = 20 mm); the results are presented in Figure 6 for case 1 and in Figure 7. Numerical and experimental results of the axial velocities for case 2 at different heights above the burner.. Near the burner exit, the velocity profiles of the inner and second jet show a constant outlet velocities. Here, the numerical and experimental results agree well. Further upstream, the velocity profiles show a greater difference, resulting in different jet lengths.

The experimental results of the Reynolds stress components (constant density) in axial and radial direction at a height of 10 mm above the burner are shown in Figure 8 for case 1. The results show a symmetric pattern of the jets. For the axial velocity component u_a, the highest values of variations (about 2 m^2/s^2) are found in the centre of the second jet at a radial position of ± 18 mm.

Two peaks are found for the radial component u_r. The inner peak between the first and the second jet show a higher value (about 1.2 m^2/s^2) than the outer peak between the second jet and the outer layer (about 0.7 m^2/s^2). The shear stress component shows opposite behaviour with larger values on the outer side. The inner jet, assuming symmetry in radial direction, indicating isotropic turbulence with a turbulence intensity of about 5 % was observed.

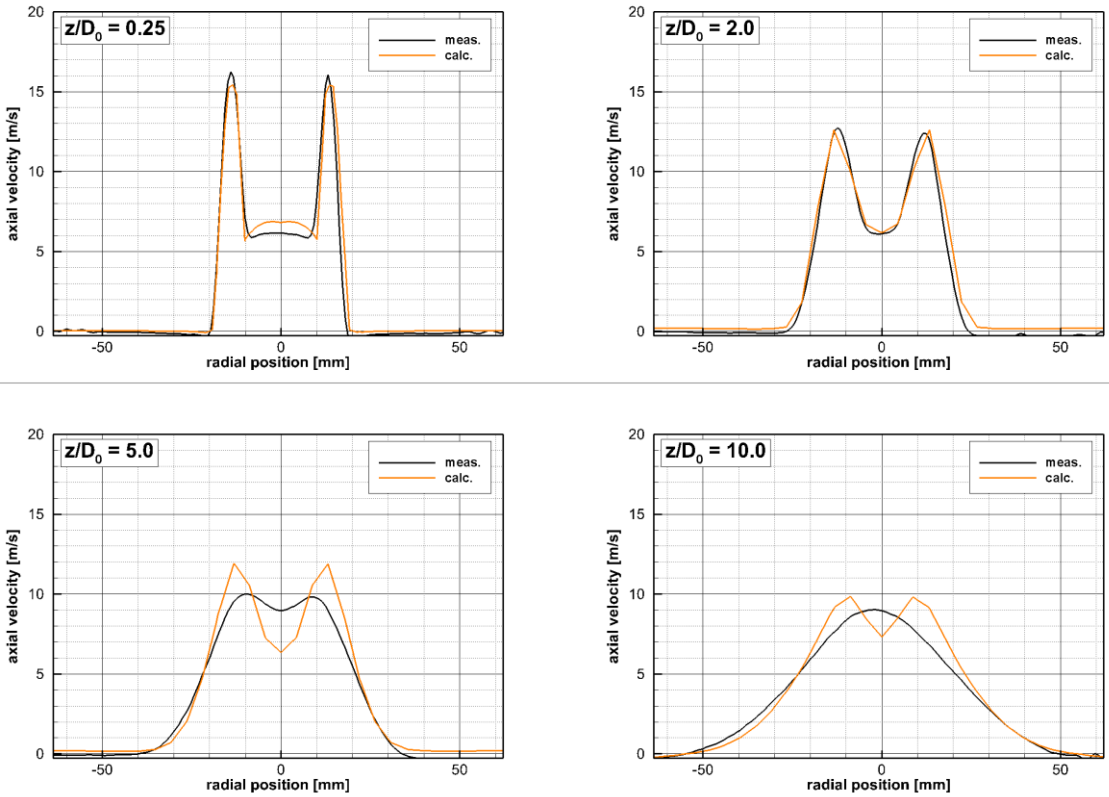

Figure 6. Numerical and experimental results of the axial velocities for case 1 at different heights above the burner.

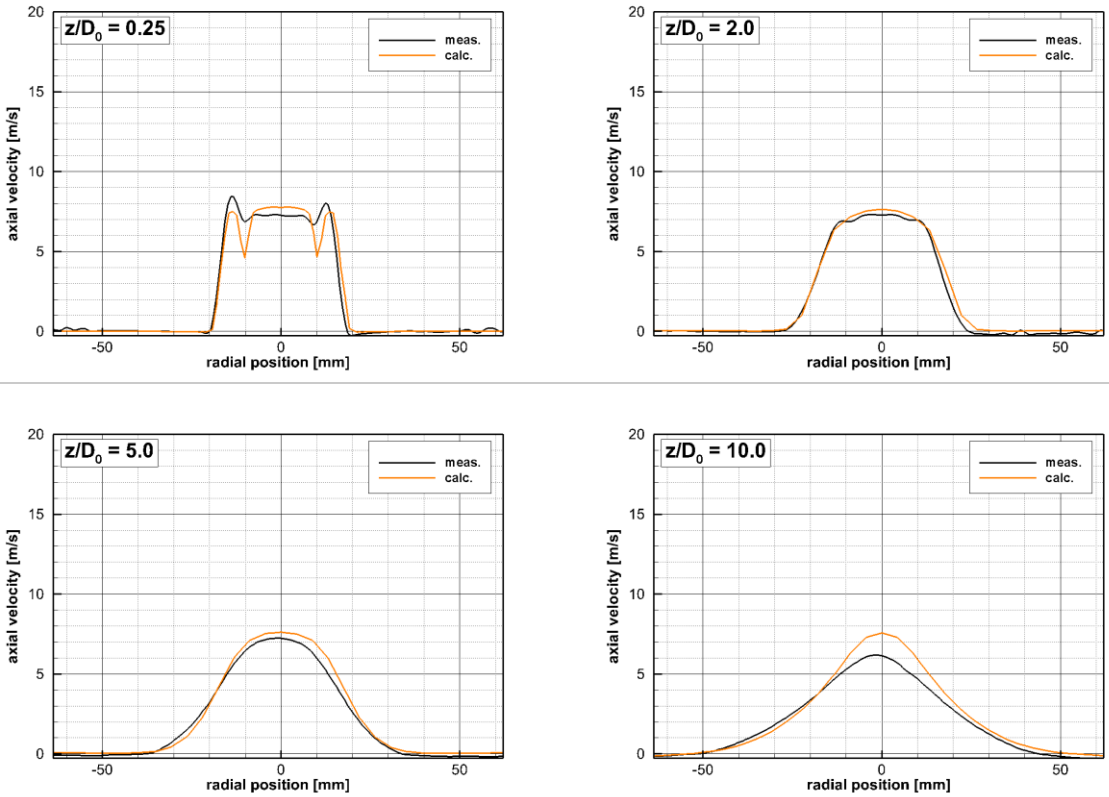

Figure 7. Numerical and experimental results of the axial velocities for case 2 at different heights above the burner.

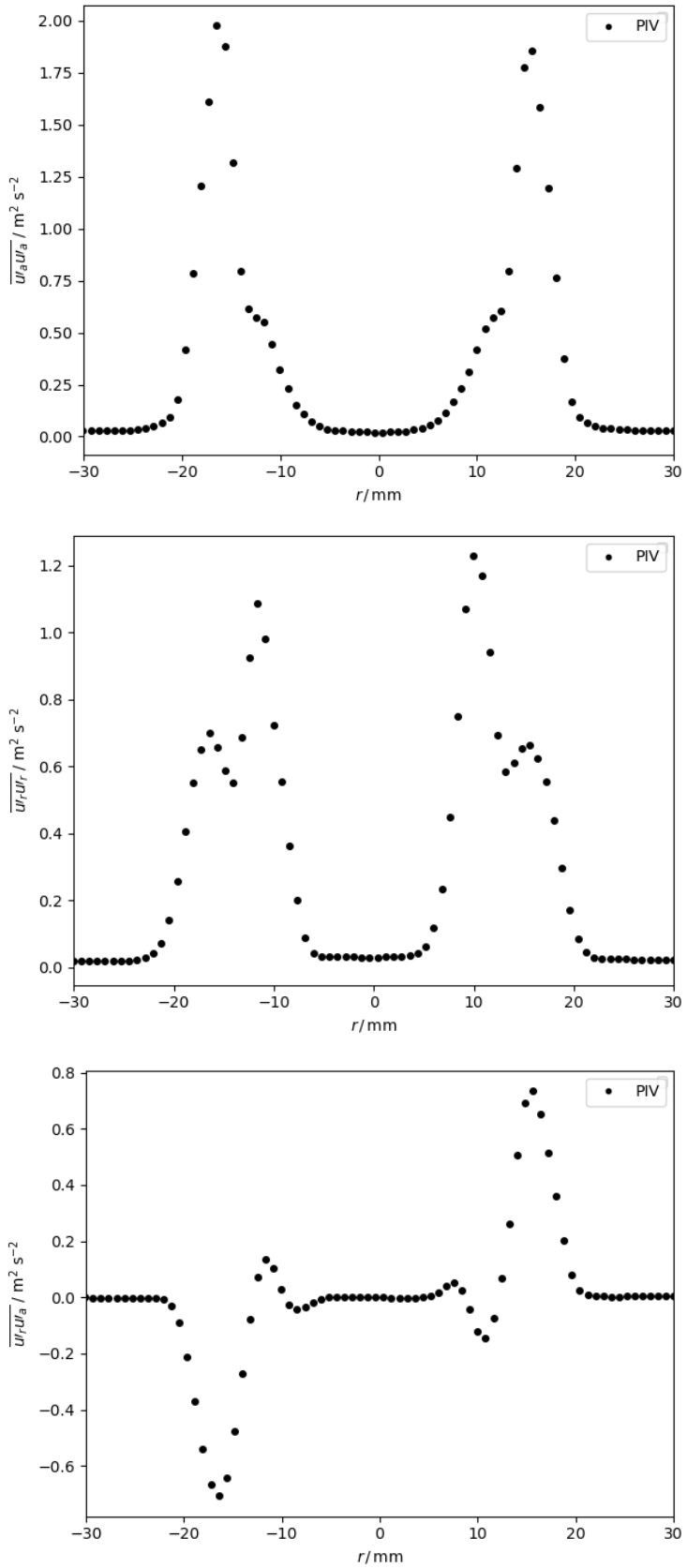

Figure 8. *The experimental results of the Reynolds stress components (constant density) in axial and radial directions and the shear stress component for case 1 at a height of 10 mm above the burner.*

Conclusions

In this paper, a model burner for turbulent premixed hydrogen-air combustion at high exhaust gas recirculation (EGR) rates was presented. In a preliminary study, the laminar burning velocities of hydrogen air flames with high EGR were investigated to identify the operating range in EGR cases. The burner design with two nozzles and a co-flow was presented and expected flame lengths were estimated.

The flow field was experimentally and numerically investigated for non-reactive conditions. The numerical and experimental results agree well, especially the expected outlet velocities of the designed nozzles near the burner exist: the results shows that the nozzle design of the inner jet and second jet lead to a constant velocity profile at the burner outlet. The analysis of the Reynolds stress and shear stress component revealed an almost isotropic turbulence with an intensity of about 5 % in this region. In addition, the two shear layers between the inner and second jet as well the second jet and the outer layer were determined. The total lengths of the jet are between 220 mm and 300 mm, with the experiments showing shorter results than the numerical simulations.

Acknowledgements

The authors would like to acknowledge the financial support by the Friedrich and Elisabeth Boysen Foundation in the project “Premixed hydrogen combustion at high recirculation rates” (BOY-178). The present research work contributes to the MTET program, Resource and Energy Efficiency, Anthropogenic Carbon Cycle (38.05.01) of Helmholtz Association. In addition, the authors would like to thank the German Research Foundation (DFG) for the financial support of measuring equipment within the HBFG program INST 121384/178-1 FUGG.

References

[1] Dreizler A., Pitsch H., Schulz C., Janicka J.: *Energiewende: verlässlich, machbar, technologieoffen*, 2020.
[2] Sharma S., Ghoshal S. K.: *Hydrogen the future transportation fuel: From production to applications*, Renewable and Sustainable Energy Reviews, 1151–8, 2015.
[3] Garcia A. M., Le Bras S., Polifke W.: *Effect of hydrogen addition on the consumption speed of lean premixed laminar methane flames exposed to combined strain and heat loss*, Combustion Theory and Modelling, 4, 584–604, 2023.
[4] Zhang W., Wang J., Lin W., Mao R., Xia H., Zhang M., Huang Z.: *Effect of differential diffusion on turbulent lean premixed hydrogen enriched flames through structure analysis*, International Journal of Hydrogen Energy, 18, 10920–31, 2020.
[5] Pareja J., Burbano H. J., Ogami Y.: *Measurements of the laminar burning velocity of hydrogen–air premixed flames*, International Journal of Hydrogen Energy, 4, 1812–8, 2010.
[6] Sivashinsky G. I.: *Instabilities, Pattern Formation, and Turbulence in Flames*, Annu. Rev. Fluid Mech., 1, 179–99, 1983.
[7] Yip H. L., Srna A., Yuen A. C. Y., Kook S., Taylor R. A., Yeoh G. H., Medwell P. R., Chan Q. N.: *A Review of Hydrogen Direct Injection for Internal Combustion Engines: Towards Carbon-Free Combustion*, Applied Sciences, 22, 4842, 2019.
[8] Vance F. H., Goey L. de, van Oijen J. A.: *Development of a flashback correlation for burner-stabilized hydrogen-air premixed flames*, Combustion and Flame, 112045, 2022.
[9] Chaichan M. T.: *Characterization of Lean Misfire Limits of Mixture Alternative Gaseous Fuels Used for Spark Ignition Engines*, Tikrit Journal of Engineering Sciences, 1, 50–61, 2022.
[10] Chaichan M. T.: *Practical study of compression ratio, spark timing and equivalence ratio effects on SIE fueled with hydrogen*, Proceeding to Industrial Applications of Energy Systems, Sohar University, Oman, 2008.
[11] Chiesa P., Lozza G., Mazzocchi L.: *Using Hydrogen as Gas Turbine Fuel*. In: Proceedings of the ASME Turbo Expo 2003: Presented at the 2003 ASME Turbo Expo, June 16 - 19, 2003, Atlanta, Georgia. New York, NY: American Society of Mechanical Engineers; 2003, p. 163–171.
[12] Lu C., Zhang L., Cao C., Chen X., Xing C., Shi H., Liu L., Qiu P.: *The effects of N2 and steam dilution on NO emission for a H2/Air micromix flame*, International Journal of Hydrogen Energy, 63, 27266–78, 2022.
[13] Shang W., Yu X., Shi W., Xing X., Guo Z., Du Y., Liu H., Wang S.: *Effect of exhaust gas recirculation and hydrogen direct injection on combustion and emission characteristics of a n-butanol SI engine*, International Journal of Hydrogen Energy, 35, 17961–74, 2020.
[14] Miqdam Tariq Chaichan: *EGR effects on hydrogen engines performance and emissions*, International Journal fo Scientific & Engineering Research, 3, 80–90, 2016.
[15] Ditaranto M., Heggset T., Berstad D.: *Concept of hydrogen fired gas turbine cycle with exhaust gas recirculation: Assessment of process performance*, Energy, 116646, 2020.

[16] Verhelst S., Vancoillie J., Naganuma K., Paepe M. de, Dierickx J., Huyghebaert Y., Wallner T.: *Setting a best practice for determining the EGR rate in hydrogen internal combustion engines*, International Journal of Hydrogen Energy, 5, 2490–503, 2013.
[17] Thomas Koch D., Sousa A., Bertram D.: *H2-Engine Operation with EGR Achieving High Power and High Efficiency Emission-Free Combustion*. In: SAE Technical Paper Series. SAE International400 Commonwealth Drive, Warrendale, PA, United States; 2019.
[18] Nande AM, Szwaja S, Naber JNande, Abhijeet M; Szwaja, Stanislaw; Naber, Jeffrey: *Impact of EGR on combustion processes in a hydrogen fuelled SI engine*; 2008.
[19] Duva B. C., Toulson E.: *Unstretched unburned flame speed and burned gas Markstein length of diluted hydrogen/air mixtures*, International Journal of Hydrogen Energy, 14, 9030–44, 2022.
[20] Wang S., Zhai Y., Wang Z., Hou R., Zhang T., Ji C.: *Comparison of air and EGR with different water fractions dilutions on the combustion of hydrogen-air mixtures*, Fuel, 124686, 2022.
[21] Driscoll J. F., Chen R.-H., Yoon Y.: *Nitric oxide levels of turbulent jet diffusion flames: Effects of residence time and damkohler number*, Combustion and Flame, 1, 37–49, 1992.
[22] Barlow R., Smith N., Chen J., Bilger R.: *Nitric oxide formation in dilute hydrogen jet flames: isolation of the effects of radiation and turbulence-chemistry submodels*, Combustion and Flame, 1-2, 4–31, 1999.
[23] Meier W., Prucker S., Cao M.-H., Stricker W.: *Characterization of Turbulent hytVAir Jet Diffusion Flames by Single-Pulse Spontaneous Raman Scattering*, Combustion Science and Technology, 4-6, 293–312, 1996.
[24] Molkov V., Saffers J.-B.: *Hydrogen jet flames*, International Journal of Hydrogen Energy, 19, 8141–58, 2013.
[25] Wu M. S., Kwon S., Driscoll J. F., Faeth G. M.: *Turbulent Premixed Hydrogen/Air Flames at High Reynolds Numbers*, Combustion Science and Technology, 1-3, 327–50, 1990.
[26] Konnov A. A.: *Yet another kinetic mechanism for hydrogen combustion*, Combustion and Flame, 14–22, 2019.
[27] von Elbe G., Mentser M.: *Further Studies of the Structure and Stability of Burner Flames*, The Journal of Chemical Physics, 2, 89–100, 1945.
[28] Raffel M, Willert CE, Scarano F, Kähler CJ, Wereley ST, Kompenhans JRaffel, Markus; Willert, Christian E; Scarano, Fulvio; Kähler, Christian J; Wereley, Steve T; Kompenhans, Jürgen: *Particle Image Velocimetry*: A Practical Guide. 3rd ed. Cham: Springer; 2018.
[29] Secchi F., Häber T., Gatti D., Schulz S., Trimis D., Suntz R., Frohnapfel B.: *Turbulent impinging jets on rough surfaces*, GAMM-Mitteilungen, 1, 2022.